Journal of Japan Association for Earthquake Engineering, Vol. 26, No. 2, 2026
[Technical Paper (Translated Paper)]

CAUSES OF LIQUEFACTION DAMAGE ON SIDEWALKS AND DAMAGE REDUCTION EFFECT DUE TO DRAINAGE

Hideyuki MANO[1] and Toshiyuki IWAI[2]

[1] Member, Dr. Eng., Manager, Construction Technology Division, Shimizu Corporation, Tokyo, Japan, mano_h@shimz.co.jp
[2] Institute of Technology, Shimizu Corporation, Tokyo, Japan, kuwata@shimz.co.jp

ABSTRACT: Centrifugal model experiments were conducted to investigate the change in pore water pressure after liquefaction under conditions where impermeable roadbeds of different thicknesses were adjacent to each other like a roadway and sidewalk. If the water film formed at the bottom of the impermeable layer during the dissipation process of excess pore water pressure due to liquefaction is continuous between the roadway and sidewalk areas, the water pressure exceeding the overburden pressure may act on the sidewalk area where the impermeable layer is thinner. This water pressure caused the ground surface of the sidewalk area to rise due to heaving. In the case where a drain was installed in the roadbed of the sidewalk area, little uplift of ground occurred.

Keywords: *Liquefaction, Heaving, Impermeable layer, Water film, Drainage, Centrifugal model test*

1. INTRODUCTION

The 2011 off the Pacific coast of Tohoku Earthquake caused extensive liquefaction damage, particularly in reclaimed areas such as Urayasu City. However, examination of the road damage revealed that even though some roadways developed cavities under the roadbed during subsequent surveys[1)], vehicle traffic was possible shortly after the earthquake and damage was relatively minor in most locations. In contrast, sidewalks suffered significant damage, such as large uplifts, as shown in Photo 1. Conversely, a large amount of sand boiling caused differential settlement, as shown in Photo 2[2)]. One possible cause of the uplift during liquefaction is the buoyancy of the buried pipes. According to Urayasu City's sewerage ledger, at both locations where sidewalk uplift occurred (Photo 1), sewer pipes were laid underneath the roadway, but not underneath the sidewalk. At Mihama 2-chome (left side of Photo 2), sewer pipes were laid underneath the roadway, but not underneath the sidewalk. At Takasu 7-chome (right side of Photo 2), sewer pipes were laid underneath both the roadway and sidewalk. Therefore, it can be concluded that the cause of the liquefaction damage occurring only on the sidewalks (and not on the roadways) at the four locations shown in the photographs is not the uplift of the buried pipes.

Since the roadway and sidewalk were adjacent, the ground conditions were identical. Therefore, the difference in damage is thought to be due to differences in the pavement and roadbed thicknesses. Hence,

in this study, centrifugal model experiments simulating the differences in the thicknesses between the roadbeds underneath the roadway and sidewalk were to clarify the cause of sidewalk damage based on changes in the water pressure after liquefaction.

(Chidori, Urayasu, captured on March 18, 2011)

(Maihama, Urayasu, captured on March 18, 2011)

Photo 1 Raised sidewalk due to liquefaction

(Mihama 2, Urayasu, captured on March 18, 2011)

(Takasu 7, Urayasu, captured on March 18, 2011)

Photo 2 Sidewalk subsidence caused by liquefaction

2. PAVEMENT STRUCTURE OF THE ROADWAY AND SIDEWALK

Figure 1 shows an example of the pavement configuration of a roadway and sidewalk on an arterial road in Urayasu City[3]. The roadway has a total thickness of 900 mm, comprising a pavement and roadbed. In contrast, the sidewalk is thinner than the roadway, with a total thickness of 200 mm. A recycled crusher run is used for the roadbed. The permeability of the roadbed decreases over time due to the self-hardening nature of recycled concrete aggregates. One report highlighted that it was impossible to conduct an in situ permeability test using a pavement permeability tester 10 months after placement[4]. Therefore, roadbeds using recycled crusher runs are considered almost impermeable to a sudden increase in water pressure such as liquefaction.

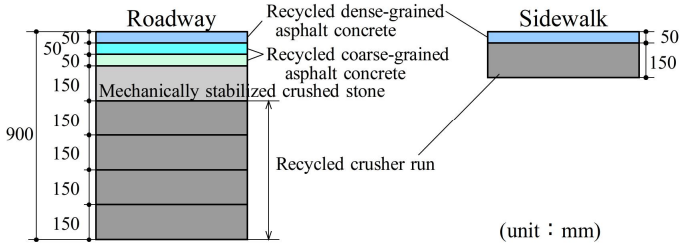

Fig. 1 Example of pavement configuration of a roadway and sidewalk[3]

3. CENTRIFUGAL MODEL EXPERIMENTS

In this study, centrifugal model experiments were conducted to investigate the changes in the pore water pressure and ground surface displacement after liquefaction under conditions where impermeable

roadbeds of different thicknesses, such as roadways and sidewalks, were adjacent to one another[5]. By comparing cases with and without roadbed permeability and with uniform roadbed thickness, the impact of sidewalk on liquefaction damage was clarified.

3.1 Description of the Centrifugal Model Experiments

Centrifugal model experiments were carried out at a centrifugal acceleration of 30 g using a laminar soil box with a length × breadth × depth of 800 mm × 230 mm × 420 mm. Silica sand no. 7 mixed with 5% of kaolin was used as the liquefiable layer and silica sand no. 3 was used as the ground material to simulate the roadbed. Silicone oil with a kinematic viscosity of 30 mm^2/s was used as the pore fluid. The physical properties of the geomaterials are listed in Table 1, and their grain size accumulation curves are shown in Fig. 2. Although both soil materials used in the experiments deviated slightly from the particle size range suitable for the maximum and minimum density tests, the values listed in Table 1 were obtained using the method specified in the JIS A 1224:2020 standard. These experiments primarily focused on post-liquefaction behavior, and therefore, the liquefaction layer was set to a density that was prone to liquefaction and ensured good reproducibility in soil preparation. However, because the roadbed is compacted during actual construction, a dense soil was created using the air pluviation method. For the experiments, an impermeable layer was created at the bottom of the roadbed by applying a 0.5-mm thick rubber sheet. Although the rubber sheet itself was impermeable, some leakage occurred at points such as the instrument cable extraction points. As described later, a rubber sheet was applied such that it was convex upward to ensure both water interception and subsidence-following capabilities.

Table 1 Physical properties of the geomaterials

Item	Silica sand no. 7 + 5% kaolin	Silica sand no. 3
Soil particle density (g/cm^3)	2.630	2.654
Mean grain size (mm)	0.140	1.520
Minimum void ratio	0.645	0.655
Maximum void ratio	1.181	0.980
Experimental condition		
Dry unit weight (kN/m^3)	12.87	15.58
Relative density (%)	33	99
Wet unit weight (Sr = 90%) (kN/m^3)	17.40	—
Saturated unit weight (kN/m^3)	17.78	19.52

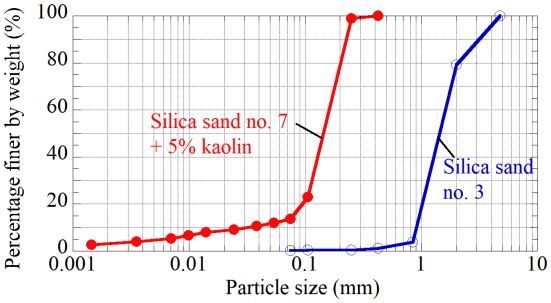

Fig. 2 Grain size accumulation curves of the geomaterials

The experimental cases are presented in Table 2 and the physical models for each case are shown in Fig. 3. Each case was different, depending on the presence or absence of a permeable roadbed, and the existence of a thin sidewalk section if the roadbed was impermeable.

The thickness of the roadbed in the roadway section was 30 mm (900 mm at the prototype scale) using silica sand no. 3. The sidewalk section was a 100-mm square in plan and enclosed within plastic formwork. For the sidewalk section, the same ground as the liquefiable layer was constructed to a thickness of 20 mm, and a rubber sheet was applied on top of the liquefiable layer. A 10-mm thick layer of silica sand no. 3 (300 mm at the prototype scale) was formed on the rubber sheet, which served as the roadbed. A brief description of each experimental case is presented below.

CASE 1: Case where there was no impermeable layer (rubber sheet) underneath the roadbed and the roadbed thickness was uniform.

CASE 2: Case where there was an impermeable layer (rubber sheet) underneath the roadbed and the roadbed thickness was uniform.

CASE 3: Case where there was an impermeable layer (rubber sheet) underneath the roadbed, and the roadway and sidewalk sections with different roadbed thicknesses were adjacent to one another.

Table 2 Experimental cases

	Presence of impermeable layer (rubber sheet)	Roadbed thickness		Installation of drain	Groundwater level (actual measurement)
		Roadway	Sidewalk		
CASE 1	No	30 mm (0.9 m)	—	—	−16 mm (−0.48 m)
CASE 2	Yes		—	—	−25 mm (−0.75 m)
CASE 3			10 mm (0.3 m)	No	−15 mm (−0.45 m)
CASE 4				Yes	−22 mm (−0.66 m)

( ): at the prototype scale

CASE 4: Case where the physical model was the same as that for Case 3, but a drain was installed in the roadbed of the sidewalk to enable drainage.

The ground formation method is outlined as follows.

(1) A 0.5-mm thick rubber sheet was suspended along the side wall of the soil box from the top of the box to a depth of 100 mm below the surface of the liquefiable layer. The bottom (50 mm) of the suspended rubber sheet was fixed to the sidewall of the soil box using a water sealant.

(2) To ensure that the silicone oil permeated uniformly during soil saturation, a 30-mm thick layer of silica sand no. 3 was constructed at the bottom of the soil box using the air pluviation method.

(3) A 300-mm thick liquefiable layer was constructed using the air pluviation method. Water pressure gauges were installed at designated positions during soil formation. After constructing the liquefiable layer, the silicone oil was allowed to permeate from the bottom in a vacuum chamber to saturate the ground.

(4) After saturation was complete, the groundwater level was lowered to the surface of the liquefiable layer. The rubber sheet was cut 50 mm above the surface of the liquefiable layer and folded inward to create a pasting margin. The water sealant was applied to the margin, and the rubber sheet was affixed to provide an impermeable surface. The rubber sheet on the surface of the liquefiable layer, which served as the impermeable surface, was pre-mounted with two pipes (inner diameter: 18 mm, length: 40 mm) serving as air holes and water level check holes. For CASE 3 and CASE 4, the formwork members for the sidewalk section were also pre-mounted. A rubber sheet was installed such that it was convex upward to ensure both water interception and subsidence-following capabilities.

(5) For CASE 3 and CASE 4, a 20-mm liquefiable layer was constructed inside the formwork for the sidewalk and the rubber sheet was laid, as described in (4). For CASE 4, a drain with an inner diameter of 13 mm was pre-mounted onto the rubber sheet at the location shown in Fig. 3. In addition, a notch was cut into the formwork to prevent silicone oil from accumulating inside.

(6) On top of the rubber sheet, a roadbed was constructed using silica sand no. 3 by the air pluviation method. The thicknesses of the roadbed were set at 30 mm (prototype scale: 0.9 m) for the roadway and 10 mm (prototype scale: 0.3 m) for the sidewalk. For CASE 4, the drain was also filled with silica sand to a thickness of 10 mm.

(7) After constructing the roadbed, the groundwater level was adjusted to approximately 30 mm below the ground surface using the water level check holes. These holes were then sealed prior to the experiment.

During ground preparation, the groundwater level was adjusted to approximately −30 mm below the ground level (GL). However, due to soil compression caused by centrifugal loading, the water levels prior to shaking were between −15 and −25 mm below the ground surface, as shown in Table 2.

The instruments were installed at the positions shown in Fig. 3. The installation depth of the pore pressure gauges (diameter: 10 mm) was set at the center of the gauges. A thin plate with a length of 50

mm was attached to the bottom of each pore pressure gauge to prevent the instruments from sinking during liquefaction. The number at the end of each pore water pressure gauge's label indicates the depth (m) from the GL at the prototype scale.

The input was a sinusoidal wave with a frequency of 2 Hz and maximum acceleration of 400 cm/s^2 at the prototype scale. The shaking times at the prototype scale were 15, 30, and 5 s for increasing, steady-state, and decreasing shaking events, respectively, for a shaking period of 50 s.

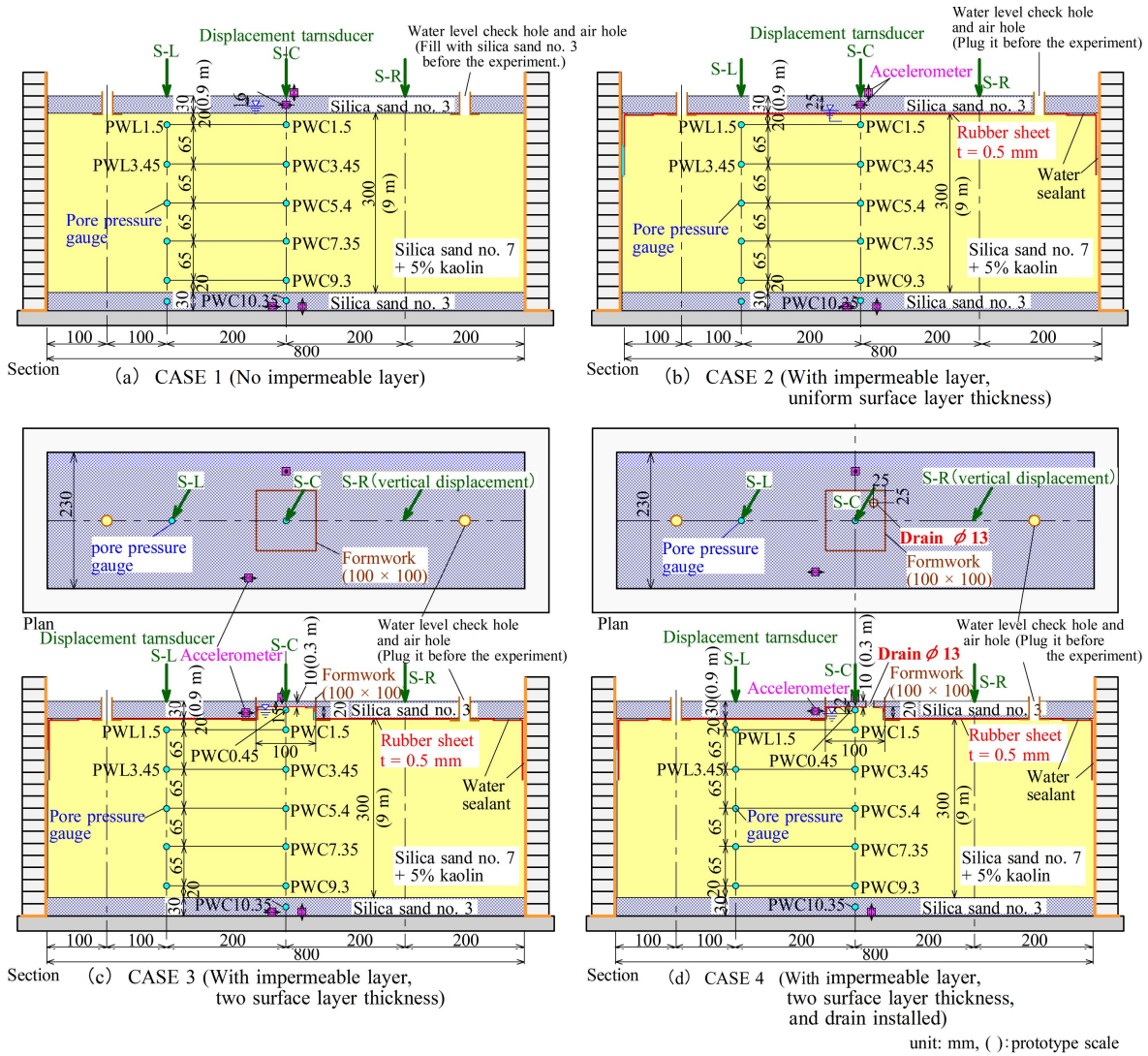

Fig. 3 Physical models for all experimental cases in this study

3.2 Experimental Results

All the experimental results are shown at the prototype scale. The acceleration waveforms of the roadbed were nearly identical across the entire set of cases, and therefore, the acceleration waveforms at the bottom of the soil box (input wave) and roadbed for CASE 4 is shown as an example (Fig. 4). Five seconds after shaking commenced, the roadbed acceleration did not increase, indicating that liquefaction had occurred.

Figures 5(a)–(d) show the time histories of the excess pore water pressure at depths shallower than

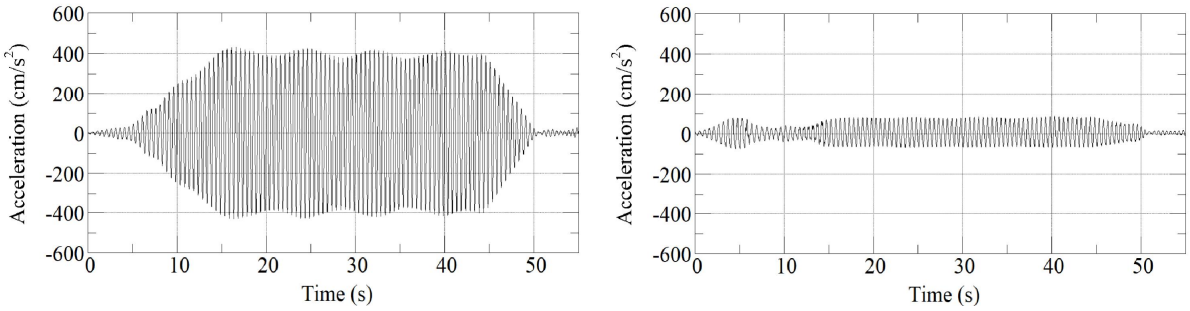

(a) Input (b) Roadbed

Fig. 4 Acceleration–time histories

GL−3.45 m, the excess pore water pressure ratio, and the vertical displacement of the ground surface after shaking had ended for each case. Because centrifugal acceleration acted in the radial direction from the center of rotation, the ground surface was concavely deformed during liquefaction, and the amount of ground surface subsidence differed between the center and edges. To eliminate this effect, the subsidence of the ground surface when shaking had ended was used as a reference. The effective stress used to calculate the excess pore water pressure ratio was calculated by considering the effect of the difference in overburden pressure between the roadway and area directly under the sidewalk using the elastic theory equation.

The results of each experimental case are described below.

CASE 1: Case where an impermeable layer (rubber sheet) was absent, and the roadbed had high permeability

Due to the high permeability of the roadbed, the excess pore water pressure ratio at GL−1.5 m (PWC1.5) only increased to approximately 0.7 immediately after shaking ended. At deeper locations, the excess pore water pressure ratio reached a value of 1 immediately after shaking ended, indicating that liquefaction had occurred. After shaking had ended, the excess pore water pressure decreased rapidly from the deeper layers. By approximately 2,000 s, the excess pore water pressure nearly dissipated throughout the entire depth. Subsidence also ceased at roughly the same time, where the final subsidence was 100–170 mm.

CASE 2: Case where an impermeable layer (rubber sheet) was present underneath the roadbed and the roadbed soil thickness was uniform

Immediately after shaking, the excess pore water pressure ratio reached a value of 1 at all depths, indicating that the entire liquefiable soil layer had liquefied. After shaking had ended, the pore water pressure decreased from the deeper layers. The excess pore water pressure increased slightly before decreasing. Shallower locations exhibited a greater increase in the water pressure over a longer duration. At an elapsed time of approximately 3,000 s, the excess pore water pressures were nearly identical at PWC1.5 and PWC3.45, or PWL1.5 and PWL3.45, which shared the same plane position but differed in depth. Subsequently, the water pressure at both locations remained equal and gradually decreased. Because the rubber sheet prevented drainage from the liquefiable layer to the roadbed, the decrease in water pressure took a longer time compared with that for CASE 1. Even after 8,000 s, the shallow-layer water pressure did not cease to decrease.

During the initial 1,500 s, almost no subsidence occurred at the ground surface. Subsequently, subsidence occurred, though it was smaller compared with that for other cases, amounting to only 50–60 mm even after an elapsed time of 8,000 s.

CASE 3: Case where an impermeable layer (rubber sheet) was present underneath the roadbed, and the roadbed thicknesses differed between the roadway and sidewalk.

The excess pore water pressure ratio immediately after shaking had ended reached a value of approximately 1 at all depths except at PWC0.45, which was in contact with the unsaturated layer. This

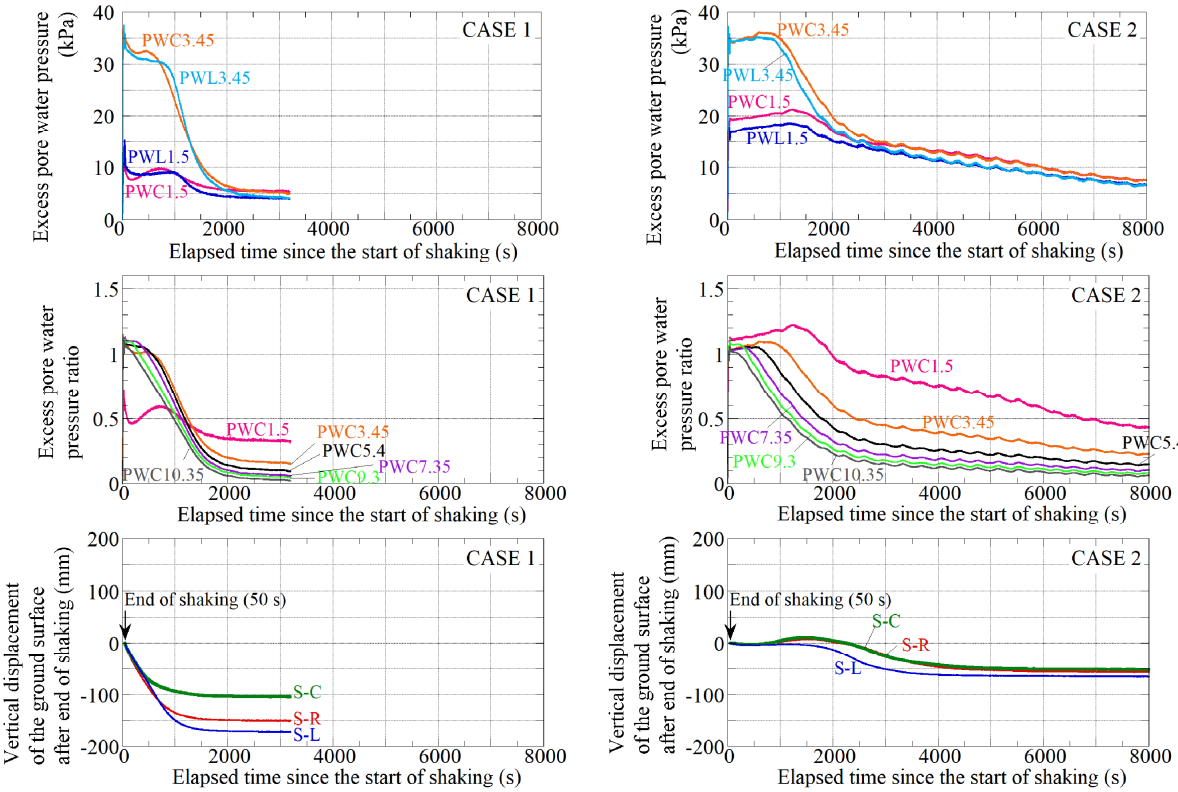

(a) CASE 1 (b) CASE 2

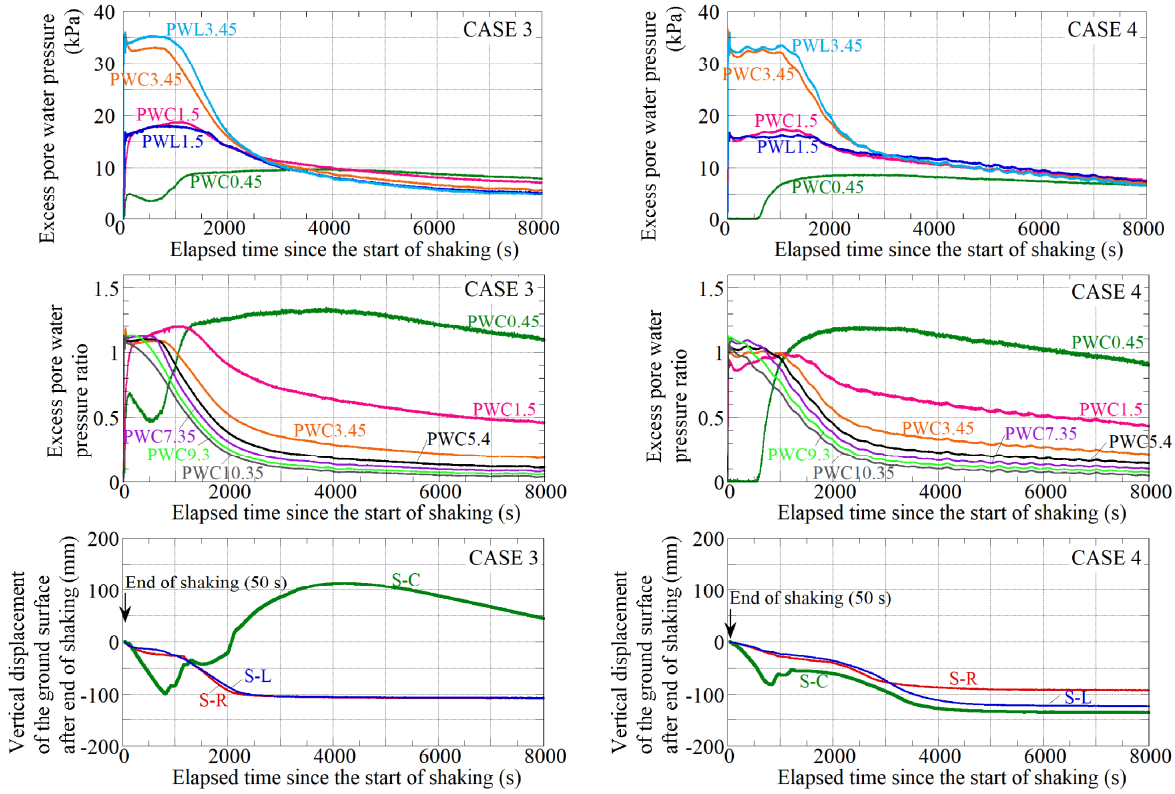

(c) CASE 3 (d) CASE 4

Fig. 5 Time histories of the excess pore water pressure, excess pore water pressure ratio, and vertical displacement of the ground surface for each experimental case

indicated that the ground deeper than the groundwater level had liquefied. After shaking had ended, the excess pore water pressure decreased from the deeper layers, similar to that for other cases. However, at GL−1.5 m, the water pressure slightly increased for approximately 1,000 s. The excess pore water pressure at PWC0.45, immediately below the sidewalk's roadbed, initially decreased after shaking had ended, but increased rapidly after 600 s. The excess pore water pressure at PWC0.45 continued to increase until an elapsed time of approximately 4,000 s, exceeding that at PWC1.5, which was deeper than PWC0.45. The excess pore water pressure ratio also increased to a maximum of 1.35, exceeding a value of 1. The excess pore water pressure then decreased; however, the excess pore water pressure in the sidewalk section remained higher at shallower depths compared with those at deeper depths. In contrast, the excess pore water pressure in the roadway section at PWL1.5 and PWL3.45 reached a nearly identical value after 3,000 s. Subsequently, the water pressures at both locations remained equal and gradually decreased, as observed for CASE 2.

The surface displacement showed a relatively small subsidence in the roadway sections (S-L and S-R) during the first 1,000 s after shaking had ended. The subsidence progressed somewhat rapidly from 800 s to 2,200 s, and then proceeded at a very slow rate. The subsidence at an elapsed time of 8,000 s was 107 mm.

However, the ground surface of the sidewalk (S-C) subsided for a short period after shaking had ended and then began to increase rapidly after an elapsed time of 800 s. After 4,000 s, the ground surface of the sidewalk was higher than that of the roadway by 271 mm.

CASE 4: Case where the physical model was the same as that for CASE 3, but a drain was installed in the roadbed of the sidewalk

At the end of shaking, the excess pore water pressure ratio was greater than 0.93 at all depths below the groundwater table, indicating that the ground deeper than the groundwater level had liquefied. The excess pore water pressure at PWC0.45 in the sidewalk increased rapidly after 600 s, as observed for CASE 3. However, the water pressure at PWC0.45 ceased to increase at about 2,500 s and never exceeded the excess pore water pressure at PWC1.5. The excess pore water pressure ratio at PWC0.45 was larger than 1, but slightly smaller than that for CASE 3, with a maximum value of 1.2.

The ground surface displacement at the sidewalk (S-C) began to increase after an elapsed time of about 800 s. However, unlike CASE 3, the uplift did not continue over a long period. At an elapsed time of approximately 1,200 s, the uplift transitioned to subsidence, and the sidewalk never rose higher than the roadway. Subsequently, the sidewalk subsided similarly to the roadway, and after 5,000 s, the subsidence nearly ceased. The final subsidence was 95–125 mm for the roadway and 135 mm for the sidewalk. The difference in subsidence between the roadway and sidewalk sections was small.

4. DISCUSSION AND REMARKS

4.1 Influence of the Roadbed Permeability (CASE 1 versus CASE 2)

Because the excess pore water pressure in the liquefiable layer was greater at deeper depths, the upward seepage flow after shaking had ended caused the excess water pressure from the deeper depths to dissipate. If the roadbed permeability was high, the pore water that rose from the deeper layers could be easily drained away, and the excess pore water pressure would decrease rapidly.

However, if the bottom of the roadbed was impermeable, the pore water could not be drained to the ground surface. Hence, the pore water accumulated just below the impermeable surface, forming a water film[6), 7)].

Therefore, a high water pressure (equal to the overburden pressure) was maintained at the bottom of the roadbed, suppressing the excess pore water pressure difference between the roadbed base and deep ground. Consequently, seepage flow from the deeper layers was also suppressed, and the decrease in the water pressure at each depth was delayed.

Without drainage from impermeable surfaces, the water film volume remains constant, and ground subsidence does not occur. However, the subsidence progressed slowly, suggesting that leakage had

occurred. The drainage volume due to the leakage was small, resulting in a smaller amount of ground surface subsidence compared with that for CASE 1. The water pressure at PWC1.5 and PWL1.5 increased by 1.81 and 1.98 kPa, respectively, within 1,200 s after shaking had ended. This was thought to be due to the consolidation of the liquefied layer, causing the instruments to subside due to the water film thickness. Based on the increase in water pressure, the water film thickness after 1,200 s was estimated to be 180–200 mm at the prototype scale (6.0–6.7 mm at the model scale).

4.2 Influence of the Presence of Sidewalk (CASE 2 versus CASE 3)

When an impermeable layer existed near the ground surface, a water film formed during the dissipation of the excess pore water pressure. When the impermeable layer thickness was uniform, the water pressure of the water film balanced the overburden pressure, and therefore, the excess pore water pressure ratio never exceeded a value of 1. Although the rate of ground surface subsidence slowed down in the absence of sand boiling, subsidence generally proceeded in a uniform manner. However, the water film was unstable and tended to form a "water passageway," flowing to the side. In previous experiments simulating sand boiling, it was confirmed that water passageways were formed from the water film to the sand boiling holes[1), 8)]. In model experiments where sites with differing degrees of compaction of the low-permeability surface layer were adjacent, the pore water flowed from the compacted side to the uncompacted side and erupted[9)]. Similarly, when roadway and sidewalk sections with different roadbed thicknesses were adjacent to one another, the water in the water film under the roadway's roadbed was expected to flow under that of the sidewalk at a shallower location during the dissipation of excess pore water pressure, forming a continuous water film between the roadway and sidewalk sections.

For CASE 3, the subsidence of the roadway sections (S-L and S-R) progressed relatively slowly for approximately 800 s after shaking had ended. Between 800 and 2,200 s, subsidence progressed somewhat rapidly, after which it proceeded slowly once again. Between 800 and 2,200 s, the water pressure at PWC0.45, located under the sidewalk's roadbed, increased sharply. Therefore, the roadway subsidence during this period was thought to have occurred because the water in the water film formed under the roadway's roadbed flowed into the space underneath the sidewalk's roadbed, causing the water film to thin by that volume. After the water pressure under the roadway and sidewalk became balanced, the flow of water from the roadway to the sidewalk ceased, and thus, the rate of roadway subsidence was thought to have slowed down once again.

Figure 6 shows a schematic of this phenomenon for CASE 3. During the dissipation of excess pore water pressure, the water in the water film underneath the thick roadway's roadbed flowed underneath the thin sidewalk's roadbed. When the water films under both roadbeds became continuous, the water pressure p_c acting under the sidewalk's roadbed increased until it balanced the water pressure p_L of the water film under the roadway's roadbed, resulting in the water pressure distribution indicated by the thick blue line on the right side of Fig. 6. The maximum value of water pressure p_c acting under the sidewalk's roadbed is expressed by Eq. (1) and the excess pore water pressure ratio $E.P.W.P.R_c$ is

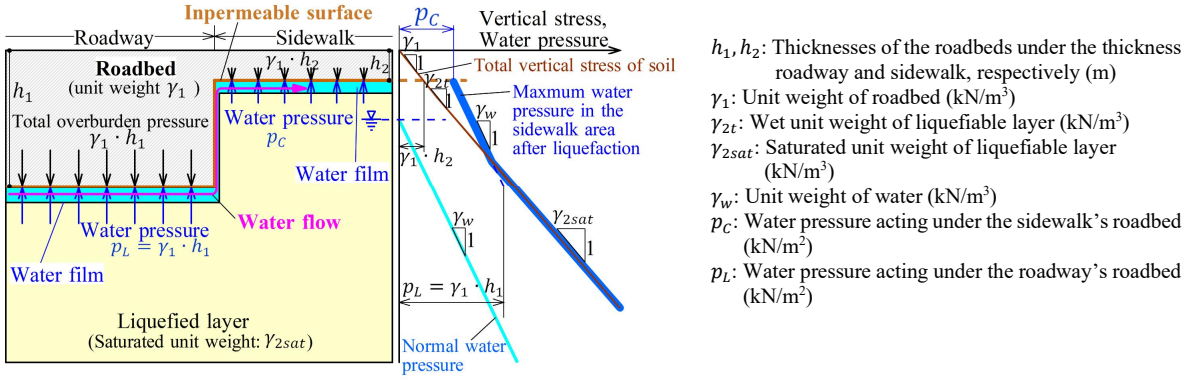

h_1, h_2: Thicknesses of the roadbeds under the thickness roadway and sidewalk, respectively (m)
γ_1: Unit weight of roadbed (kN/m^3)
γ_{2t}: Wet unit weight of liquefiable layer (kN/m^3)
γ_{2sat}: Saturated unit weight of liquefiable layer (kN/m^3)
γ_w: Unit weight of water (kN/m^3)
p_C: Water pressure acting under the sidewalk's roadbed (kN/m^2)
p_L: Water pressure acting under the roadway's roadbed (kN/m^2)

Fig. 6 Schematic of the water pressure distribution when the water film is continuous

expressed by Eq. (2). The symbols used in these equations are shown in Fig. 6.

$$\begin{aligned} p_C &= p_L - \gamma_w(h_1 - h_2) \\ &= \gamma_1 h_1 - \gamma_w(h_1 - h_2) \\ &= \gamma_1 h_2 + (\gamma_1 - \gamma_w)(h_1 - h_2) \end{aligned} \quad (1)$$

$$E.P.W.P.R_C = 1 + \frac{(\gamma_1 - \gamma_w)(h_1 - h_2)}{\gamma_1 h_2} \quad (2)$$

Based on Eqs. (1) and (2) and the maximum water pressure distribution shown in Fig. 6, the maximum excess pore water pressure and excess pore water pressure ratio at PWC0.45 for CASE 3 were determined to be 9.6 kPa and 1.32, respectively, which were in good agreement with the experimental results shown in Fig. 5(c). The maximum value of the excess pore water pressure ratio at the bottom of the sidewalk's roadbed (GL−0.3 m) was 1.74 and the safety factor for protection against heaving was 0.57, which was significantly lower than 1. The uplift of the sidewalk for CASE 3 was caused by heaving due to the water pressure.

4.3 Effectiveness of drain installed in the roadbed of the sidewalk (CASE 3 versus CASE 4)

When the roadbed thicknesses differed between the roadway and sidewalk, as described in the previous section, water pressure exceeding the overburden pressure might act under the sidewalk's roadbed, potentially causing heaving. CASE 4 demonstrated the effect of drainage in preventing heaving of the sidewalk. As shown in Fig. 5(d), the excess pore water pressure ratio at the bottom of the sidewalk's roadbed exceeded a value of 1. However, unlike CASE 3, the excess pore water pressure at PWC0.45 did not exceed those at deeper levels, and the water pressure began to decrease early because of drainage of water from the drain. Therefore, the uplift of the sidewalk was small, and the final subsidence of the sidewalk was not significantly different from that of the roadway.

4.4 Causes and Countermeasures for Sidewalk Damage Due to Liquefaction

Based on the experimental results, when sections with different roadbed thicknesses (impermeable layers) such as roadways and sidewalks were adjacent, water pressure exceeding the overburden pressure might act on the thinner roadbed of the sidewalk. In such cases, heaving was expected to occur on the sidewalk, resulting in uplift, as shown in Photo 1. In contrast, if cracks developed in the roadbed during the heaving process or if there were relative weaknesses at the boundary between the roadway and sidewalk, the high water pressure acting underneath the sidewalk's roadbed could cause piping, resulting in sand boiling. When drainage pathways to the ground surface were created by sand boiling, the increase in water pressure under the sidewalk's roadbed was suppressed, and no uplift due to heaving occurred, as observed for CASE 4. However, unlike drains that discharged only water, sand boiling discharged both the soil material and water to the ground surface. Consequently, subsidence was equivalent to the volume of the discharged soil material. It was presumed that the amount of discharged soil material increased with an increase in proximity to the sand boiling holes. Therefore, a significant differential settlement occurred on the sidewalk, as shown in Photo 2.

As described above, a water film formed underneath the roadway's roadbed during the dissipation of pore water pressure after liquefaction. Water pathways formed from the roadway to the sidewalk, allowing the water film to become continuous. Consequently, water pressure exceeding the overburden pressure acted underneath the sidewalk's roadbed. This high water pressure was believed to cause heaving and sand boiling, leading to severe liquefaction damage on the sidewalk. It takes a certain amount of time for these phenomena to manifest after liquefaction occurs. Therefore, liquefaction damage occurs after a certain period following an earthquake.

For the experiments, the groundwater level was set to be near the bottom of the roadway's roadbed.

However, even when the groundwater level is deeper and an unsaturated layer exists underneath the roadbed, the pore water can permeate from the liquefied layer to the unsaturated layer, increasing the water pressure in the unsaturated layer[10)–13)]. Under conditions where the groundwater level is high, the liquefaction layer is thick, and sufficient pore water is supplied to the unsaturated layer, and phenomena like those observed in these experiments are expected to occur even if a thin unsaturated layer exists underneath the roadbed. Liquefaction damage is particularly pronounced on sidewalks compared with that on thin roadbeds. Hence, it is believed that installing a drain in the roadbed of the sidewalk to discharge only water to the ground surface is a highly effective strategy to reduce liquefaction damage.

5. CONCLUSION

In this study, centrifugal model experiments were conducted to investigate the changes in pore water pressure and ground surface displacement over time after an earthquake for adjacent roadways and sidewalks with different impermeable roadbed thicknesses. The following conclusions were drawn based on the key findings of this study:

(1) When roadways and sidewalks with different roadbed thicknesses were adjacent to one another, the water film formed underneath the roadway's roadbed during the dissipation of excess pore water pressure after liquefaction might flow underneath the sidewalk's roadbed. In this case, the water pressure of the water film underneath the sidewalk's roadbed was balanced by that of the water film underneath the roadway's roadbed, resulting in a water pressure greater than the overburden pressure acting on the sidewalk's roadbed. This might have caused the sidewalk's roadbed to heave.

(2) No significant uplift occurred for the case where a drain was installed in the sidewalk area. Hence, the installation of a drain in the sidewalk area for drainage of only water may be highly effective in reducing liquefaction damage.

REFERENCES

1) Sera, Y., Koike, Y., Kuwano, R. and Kuwano, J.: Sub-Surface Cavities in the Liquefied Ground Caused by the Great East Japan Earthquake, *Japanese Geotechnical Journal*, Vol. 9, No. 3, pp. 323–339, 2014 (in Japanese).
2) Yasuda, S., Harada, K. and Ishikawa, K.: Damage to Structures in Chiba Prefecture During the 2011 Tohoku-Pacific Ocean Earthquake, *Japanese Geotechnical Journal*, Vol. 7, No. 1, pp. 103–115, 2012 (in Japanese).
3) Urayasu City Liquefaction Countermeasures Technical Study Investigation Committee: *2011 Urayasu City Liquefaction Countermeasures Technical Study Report*, 2012 (in Japanese).
4) Mitamura, K., Kumagai, M., and Abe, R.: Application of Recycled Concrete Aggregate to Roadbed Drainage and Intercepted Drainage, *54th Hokkaido Development Technical Research Presentation*, 2011 (in Japanese).
5) Mano, H. and Iwai, T.: Heaving Caused by Liquefaction, *58th Japan National Conference on Geotechnical Engineering*, 11-8-4-01, 2023 (in Japanese).
6) Kokusho, T., Sawano, T., Kawai, R. and Sugiyama, K.: Study on Formation of Water Film Affecting Lateral Flow of Liquefied Sand Ground, *Proceedings of the Symposium on the Fluidity and Permanent Deformation of Ground and Earth Structures during Earthquakes*, Japanese Geotechnical Society, pp. 317–320, 1998 (in Japanese).
7) Kokusho, T.: Mechanism for Water Film Generation and Lateral Flow in Liquefied Sand Layer, *Soils and Foundations*, Vol. 40, No. 5, pp. 99–111, 2000.
8) Numata, A. and Someya, N.: Grain Size Distribution of Erupted Soil Due to Liquefaction Using Simplified Shaking Test, *34th Japan National Conference on Geotechnical Engineering*, pp. 2079–2080, 1999 (in Japanese).
9) Yamaguchi, A., Yoshida, N. and Tobita, Y.: Estimation of Thickness of Liquefied Layer from Sand Boiling Pattern, *Journal of Japan Society of Civil Engineers C*, Vol. 64, No. 1, pp. 79–89, 2008 (in Japanese).

10) Uzuoka, R., Kubo, T. Yashima, A. and Zhang, F.: Liquefaction Analysis with Seepage to Partially Saturated Surface Soil, *Journal of Japan Society of Civil Engineers*, No. 694, pp. 153–163, 2001 (in Japanese).
11) Takada, Y. Ueda, K., Mikami, T. and Iai, S.: Liquefaction Behavior of Sandy Ground Focusing on Pore Water Inflow into Partially Saturated Surface Layer, *52nd Japan National Conference on Geotechnical Engineering*, pp. 833–834, 2017 (in Japanese).
12) Ishikawa, K. Yasuda, S. and Nagai, S.: Deformation Behavior of the Spread-Foundation Structure Due to the Dissipation of the Excess Pore Water Pressure, *53rd Japan National Conference on Geotechnical Engineering*, pp. 1231–1232, 2018 (in Japanese).
13) Kawamata, Y., and Iijima, M.: Infiltration of Pore Water into the Surface Unsaturated Layer During Liquefaction and Its Effects, *Japan Society of Civil Engineers 2020 Annual Meeting*, III-118, 2020 (in Japanese).

(Original Japanese Paper Published: November, 2024)
(English Version Submitted: January 9, 2026)
(English Version Accepted: February 10, 2026)